Journal of Neuroinflammation

RESEARCH

Open Access

Ketogenic diet modulates immune cell transcriptional landscape and ameliorates experimental autoimmune uveitis in mice

Runping Duan[1†], Tianfu Wang[1†], Zhaohuai Li[1†], Loujing Jiang[1†], Xiaoyang Yu[2†], Daquan He[1], Tianyu Tao[1], Xiuxing Liu[1], Zhaohao Huang[1], Lei Feng[3*] and Wenru Su[4,1*]

Abstract

Background Uveitis manifests as immune-mediated inflammatory disorders within the eye, posing a serious threat to vision. The ketogenic diet (KD) has emerged as a promising dietary intervention, yet its impact on the immune microenvironments and role in uveitis remains unclear.

Methods Utilizing single-cell RNA sequencing (scRNA-seq) data from lymph node and retina of mice, we conduct a comprehensive investigation into the effects of KD on immune microenvironments. Flow cytometry is conducted to verify the potential mechanisms.

Results This study demonstrates that KD alters the composition and function of immune profiles. Specifically, KD promotes the differentiation of Treg cells and elevates its proportion in heathy mice. In response to experimental autoimmune uveitis challenges, KD alleviates the inflammatory symptoms, lowers $CD4^+$ T cell pathogenicity, and corrects the Th17/Treg imbalance. Additionally, KD decreases the proportion of Th17 cell and increases Treg cells in the retina. Analysis of combined retinal and CDLN immune cells reveals that retinal immune cells, particularly $CD4^+$ T cells, exhibit heightened inflammatory responses, which KD partially reverses.

Conclusions The KD induces inhibitory structural and functional alterations in immune cells from lymph nodes to retina, suggesting its potential as a therapy for uveitis.

Keywords Ketogenic diet (KD), Immune microenvironment, Uveitis, Experimental autoimmune uveitis (EAU)

Background

Dietary interventions have swiftly gained popularity for enhancing human health and serving as alternative treatments for various diseases. A ketogenic diet (KD), characterized by a high-fat, low-carb composition, was initially employed to treat intractable epilepsy due to its neuroprotective properties and later revealed promising therapeutic potential for a spectrum of conditions from obesity to malignancies [1, 2]. Recent studies have further highlighted KD as a promising therapeutic approach for several immune-mediated disorders [3], such as childhood intractable epilepsy [4] and colitis [5]. However, the changes in immune

†Runping Duan, Tianfu Wang, Zhaohuai Li, Loujing Jiang and Xiaoyang Yu have authors contributed equally.

*Correspondence:
Lei Feng
leifeng@zju.edu.cn
Wenru Su
swrth@163.com
[1] State Key Laboratory of Ophthalmology, Zhongshan Ophthalmic Center, Sun Yat-Sen University, Guangdong Provincial Key Laboratory of Ophthalmology and Visual Science, Guangdong Provincial Clinical Research Center for Ocular Diseases, Guangzhou 510060, China
[2] Guangzhou University of Chinese Medicine, Guangzhou 510060, China
[3] Eye Center, The Second Affiliated Hospital, Zhejiang University School of Medicine, Hangzhou 310009, China
[4] Department of Ophthalmology, Ninth People's Hospital, Shanghai Jiao Tong University School of Medicine, Shanghai, China

microenvironments following KD treatment have not been adequately elucidated.

Uveitis manifests as immune-mediated inflammatory disorders within the eye, posing a serious threat to vision [6]. It is also an autoimmune disease affecting central nervous system (CNS), differing from other organs or tissues owing to the relative immune privilege [7]. The disrupted Th17 and Treg cell homeostasis stands as the pivotal mechanism of various autoimmune conditions, including uveitis [8–11]. However, the exact mechanisms of this imbalance remain unclear. At present, corticosteroids, immunosuppressants and biologics persist as the primary treatments for uveitis, but they encounter significant hurdles, including serious systemic side effects, limited efficacy and a nonspecific nature [12–14]. Consequently, there is a pressing need for the development of new therapeutic options for uveitis. Meanwhile, the role and mechanism of KD in uveitis remain unclear.

Lymph nodes (LNs) are crucial sites for activating T cells and initiating autoimmune responses [15–17]. Autoimmune effector T cells from LNs migrate to target organs, mediating inflammation and tissue damage [18, 19]. Among these LNs, cervical draining lymph nodes (CDLNs) hold particular significance as major CNS-draining lymph nodes [20]. Experimental autoimmune uveitis (EAU) is a classical and widely used animal model for studying uveitis, closely mirroring experimental autoimmune encephalomyelitis (EAE) in pathogenic mechanisms [21]. Removing CDLNs before inducing EAE significantly reduces disease severity [22]. In uveitis, pathogenic T cells migrate from LNs to the retina under the stimulation of self-antigens or infection, initiating the disease [23]. Recent studies have reported the presence of lymphatic drainage systems in the eye, with draining function to the CDLNs through lymphatic vasculature in the optic nerve sheath [24]. However, the impact of KD on immune cell interactions between LNs and retina has not be defined.

In this study, we have constructed an immune cell atlas of CDLNs and retina from KD-treated mice, using scRNA-seq. Our findings discover that KD induces significant immunological changes. Specifically, KD reduces the proportion of T cells and inhibits pathways related to autoimmunity in healthy mice, and markedly promotes Treg differentiation. Using the animal model of uveitis, we observe that KD mitigates EAU progression by restoring the Th17/Treg balance and reducing $CD4^+$ T cell pathogenicity. In the retina, KD also led to a decline in Th17 cell proportion and an elevation in Treg. Analysis of the combined retinal and CDLN immune cells reveal that retinal immune cells, particularly $CD4^+$ T cells, exhibit heightened inflammatory responses, which KD could partially counteract. Collectively, our findings provide a comprehensive insight into the impact of KD on immune system, and propose KD as a potential therapy for uveitis.

Results

Ketogenic diet induces complicated and extensive changes in the immune profile of CDLNs

To evaluate the impact of ketogenic diet (KD), mice were evenly matched and then randomly allocated into two dietary cohorts: the normal diet (ND) and KD groups (Fig. 1a). Throughout the observation period, no significant difference in body weight (Fig. 1b) was observed between ND and KD group, indicating a comparable baseline nutritional status in both sets.

EAU model was induced by the uveitogenic retinal protein, $IRBP_{1-20}$. On day 14 after immunization, we conducted scRNA-seq on the immune cells from CDLNs of four groups: normal diet healthy control (NDC), ketogenic diet heathy control (KDC), normal diet EAU (NDE) and ketogenic diet EAU (KDE) (Fig. 1c). We firstly explored the impact of KD on healthy mice. Employing classical lineage markers [25–27], we identified eight major immune cell types, including T cells, B cells, neutrophils (Neu), monocytes (Mono), macrophages (Macro), classical

(See figure on next page.)

Fig. 1 Ketogenic diet induced complicated and extensive changes in the immune profile of CDLNs. **a** Daily diet composition during the normal diet (ND) and ketogenic diet (KD) stages respectively, represented in percent calories. **b** Changes in body weight of mice fed with ND or KD throughout the study protocol. **c** Schematic of the experimental design for single-cell RNA sequencing (scRNA-seq). CDLNs and retinas were harvested from the normal diet healthy control (NDC), ketogenic diet heathy control (KDC), normal diet EAU (NDE) and ketogenic diet EAU (KDE) group. Samples were processed via scRNA-seq by using the 10 × Genomics platform. IRBP1-20: Interphotoreceptor retinoid-binding protein 1–20. **d** Uniform manifold approximation and projection (UMAP) plot: the left showing the cluster of cell types, the right showing sample distribution across two groups. Neu, neutrophils; Macro, macrophages; Mono, monocytes; cDC, classical dendritic cells; pDC, plasmacytoid dendritic cells; NK, natural killer cells. **e** Pie charts chart showing the percentages of the immune cells derived from scRNA-seq data. **f** Number of DEGs between KDC and NDC group within each cluster projected onto the UMAP plot. **g** Volcano plot showing upregulated and downregulated DEGs of total immune cells in the KDC/NDC comparison group. **h-i** GO terms and KEGG pathways enriched in upregulated (**H**) and downregulated (**I**) DEGs of total immune cells in the KDC/NDC comparison group. Significance was calculated based on the accumulative hypergeometric distribution by Metascape webtool

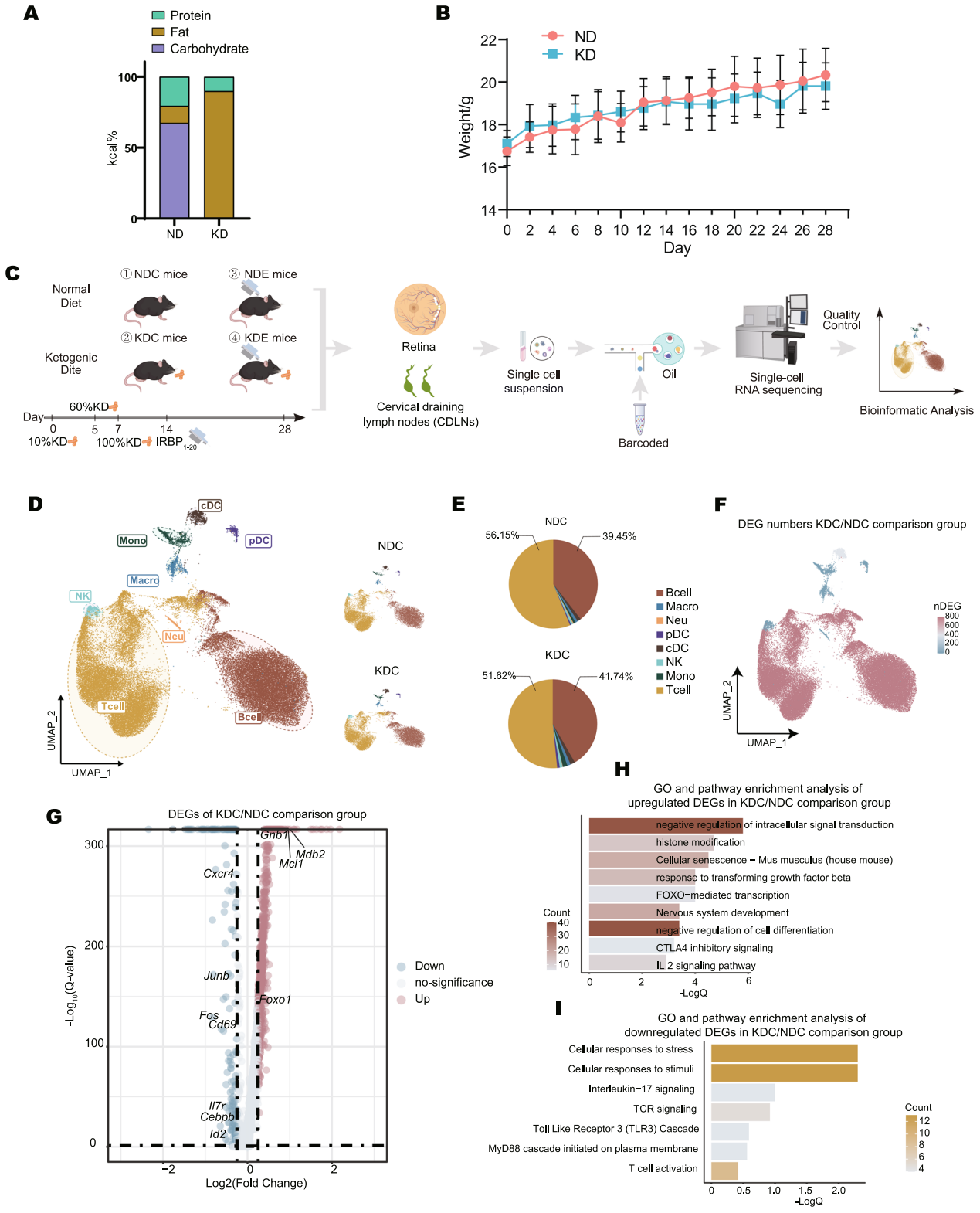

Fig. 1 (See legend on previous page.)

dendritic cells (cDC), plasmacytoid dendritic cells (pDC) and natural killer cells (NK) (Fig. 1d; Fig. S1a-b). The proportion of T cells showed reduction when transitioning to a KD (Fig. 1e).

To identify the gene signature alterations caused by KD, we performed a DEG analysis. Initially, we quantified the numbers of DEGs, noting their predominance in T and B cells (Fig. 1f). Subsequently, we explored the regulation of specific gene expression. KD was found to downregulate inflammation-related genes (*Fos* and *Junb*, both of the AP-1 family) [28], autoimmune disease-related genes (*Cebpb* and *Id2*) [29] and lymphocyte activation-related genes (*Cxcr4*, *Il7r*, and *CD69*) [30]. Meanwhile, genes related to Stat1/IFN-γ pathway inhibition (*Mbd2*) [31], apoptosis (*Mcl1*) [32] and T cell stemness (*Foxo1*) [33] were upregulated (Fig. 1g). When compared to the NDC, KDC group exhibited a lower glycolysis score and a higher AMPK signaling pathway score (Fig. S1c-d). In addition, the TGF-β signaling pathway score was increased across most cell subtypes in the KDC (Fig. S1e). Gene function analysis of all immune cells revealed that pathways related to the negative regulation of intracellular signal transduction, histone modification, cellular senescence and FOXO-mediated transcription were upregulated in response to KD (Fig. 1h); and pathways related to cellular responses to stress, TCR signaling and IL-17 signaling were downregulated (Fig. 1i). When attributed to each cell subset, pathways related to mechanisms associated with pluripotency, IL-2 signaling were upregulated (Fig. S1f) across a broad range of cell types; and pathways of neurodegeneration, cellular responses to stress, leukocyte activation, lymphocyte activation were downregulated (Fig. S1g). Overall, these findings suggested that KD may suppress the inflammation- or immune activation-related genes and pathways at baseline, particularly in T cells, highlighting its potential therapeutic benefits.

Ketogenic diet triggers functional changes of T cell and promotes Treg differentiation

Given the aforementioned findings that emphasized the impact of KD on T cells and the well-documented pivotal role of T cells in uveitis, we further re-clustered T cells into nine subsets, including naïve $CD4^+$ T cells (NCD4), regulatory T cells (Treg), T helper 17 cells (Th17), proliferative T cells (ProT), T helper 1 cells (Th1), T follicular helper cells (Tfh), γδT cells (γδT), naïve $CD8^+$ T cells (NCD8) and $CD8^+$ T cells with cytotoxic activity (CTL) (Fig. 2a, Fig. S2a-b). The DEG numbers caused by KD were predominant in Treg, CTL and NCD4 (Fig. 2b), and the upregulated genes was exclusively most in Treg cells (Fig. S2c), including genes that maintain stability (*Nrp1*) [34], promote cell differentiation (*Maf*, *Orai1*) [35, 36] and Treg inhibitory effects (*Pvt1*) [37] (Fig. 2c). Gene function analysis of Treg cells unveiled several inhibitory pathways were upregulated in KDC group, such as T cell receptor signaling pathway, signaling by TGF−beta receptor complex, FOXO−mediated transcription, and CTLA4 inhibitory signaling (Fig. 2d). Meanwhile, genes specifically downregulated in ProT cells accounted for the largest proportion (Fig. S3a), including cell cycle regulatory genes (*Ccnb2*, *Ccnd2*, *Cdk4*, *Cenpa*, *Mcm7* and *Psmd7*) (Fid. S3B). The corresponding pathways related to cell cycle were also downregulated (Fig. S3c). These results suggested KD may enhance inhibition function of Treg, while inhibit the proliferation of T cells.

Next, we performed trajectory analysis to clarify the developmental relationships of $CD4^+$ T cells during KD. Ordering of cells in pseudotime arranged most of NCD4, Teff (Th17, Th1 and Tfh) and Treg into an initial trajectory (NCD4-branch) and two bifurcations (Teff-cell fate and Treg-cell fate), respectively. We observed a pseudotemporal path started from NCD4 to Teff and Treg (Fig. 2e). Compared to the NDC group, the KDC group showed an increased ratio of Treg-cell fate, with a merely unchanged ratio of Teff-cell fate (Fig. 2f). By flow cytometry, KD didn't influence the proportions of Th1 and

(See figure on next page.)

Fig. 2 Ketogenic diet triggered functional changes of T cell and promoted Treg differentiation. **a** UMAP plot of T cell subsets: the left showing the clusters of all T cell, the right showing sample distribution across KDC and NDC groups. **b** Wind rose diagram showing the numbers of upregulated and downregulated DEGs in the KDC/NDC comparison group. **c** Violin plots showing the expression levels of *Nrp1*, *Maf*, *Pvt1*, *Orai1* in T cells. **d** GO terms and KEGG pathways enriched in upregulated DEGs of Treg cells in the KDC/NDC comparison group. Significance was calculated based on the accumulative hypergeometric distribution by Metascape webtool. **e** Pseudotime trajectory analysis of $CD4^+$ T cells. Cells are colored by pseudotime (left), celltype (middle) and state (right) as indicated. Teff: Th17, Th1, Tfh. **f** Bar charts showing the percentages of different states between NDC and KDC groups, based on the pseudotime analysis. **g-i** Proportions of Th17 cells (**G**), Th1 cells (**H**) and Treg cells (**I**) in CDLNs measured by flow cytometry, gated on $CD4^+$T cells. Data expressed as mean ± SD. Significance was determined using unpaired two-tailed student's t test. ns $P > 0.05$, ***$P < 0.001$. **j** The Treg differentiation rates of NCD4 between NDC and KDC group, measured by flow cytometry, gated on $CD4^+$T cells. Data expressed as mean ± SD. Significance was determined using one-way ANOVA. ****$P < 0.0001$. NCD4: naïve $CD4^+$ T cells, Treg: regulatory T cells, Th17: T helper 17 cells, ProT: proliferative T cells, Th1: T helper 1 cells, Tfh: T follicular helper cells, γδT: γδT cells, NCD8: naïve $CD8^+$ T cells, CTL: $CD8^+$ T cells with cytotoxic activity

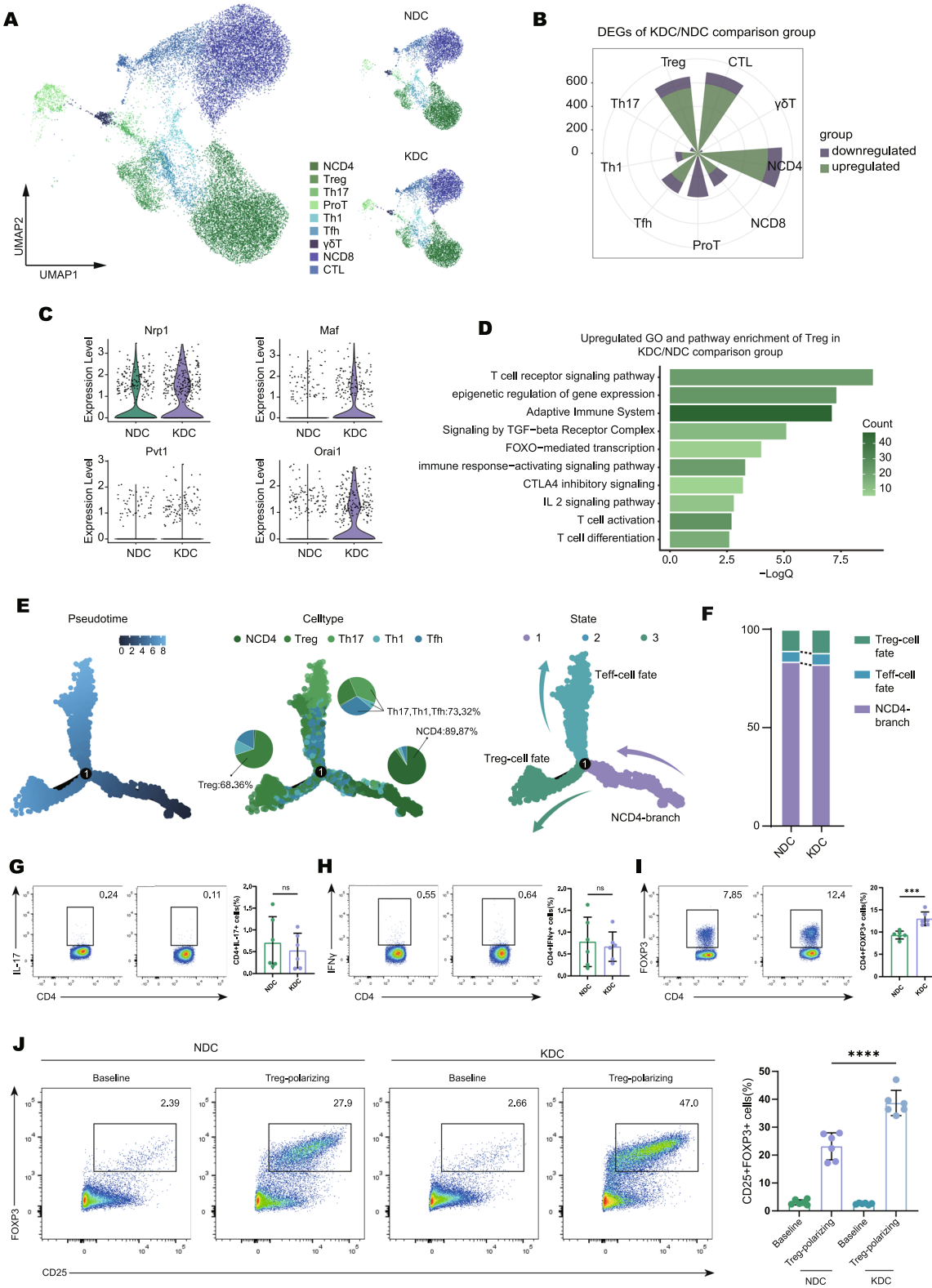

Fig. 2 (See legend on previous page.)

Th17 cells, whereas significantly increase the Treg cells (Fig. 2g–i), indicating that KD may promote Treg differentiation. To validate this hypothesis, NCD4 cells were isolated from both NDC and KDC mice, and then cultured under Treg-polarizing conditions for 72 h. Notably, the KDC group displayed a higher rate of Treg differentiation (Fig. 2j). Collectively, these findings suggest that KD treatment can promote Treg differentiation.

Ketogenic diet induces changes in B cell transcriptional profile and immune cell–cell communications

For a comprehensive illustration of KD's impact, we further re-clustered B cells into three subsets, including naïve B cells (NBC), germinal B cells (GBC), plasma B cells (PBC) (Fig. 3a, Fig. S4a-b). By SCENIC (Single Cell Regulatory Network Inference and Clustering), the transcription factor (TF) regulatory networks were predicted to determine how KD regulates B cell transcriptional profiles. Among the top 10 TFs of the two group: autoimmune related regulator, *Junb* and *Cebpb*, showed decreased transcriptional activity in KDC mice, while *Bcl11a* and *Rfx7* (DNA repair and anti-apoptosis regulatory molecule [38, 39]) displayed elevation (Fig. 3b). In addition, DEG analysis of NBCs revealed that genes associated with inflammation (*Cd24a*, *Cxcr4*, *Id2*, *Cd69* and *Cebpb*) [40], MAPK signaling pathway (*Junb*, *Fos*, *Dusp1*), glycolysis regulatory (*Myc*) [41] and immunoglobulin (*Igkc*, *Ighm*) were downregulated in the KDC group (Fig. 3c). Pathways related to T or B cell activation, differentiation, and signaling were downregulated (Fig. 3d).

Secondly, we compared the relative regulon activity of myeloid cells: the regulators related to autoimmune disease (*Irf5*), oxidative stress (*Klf9*) and macrophage activity (*Bhlhe40*) were decreased in KDC group (Fig. S4c). DEG numbers were exclusively most in cDC cells, whatever upregulated or downregulated in KDC group (Fig. S4d). Therefore, we performed gene function analysis of cDC cells. The downregulated DEGs in KDC were enriched in pathways related to neutrophil degranulation, antigen processing and presentation and mononuclear cell migration, while the upregulated are related to negative regulation of immune system process and leukocyte cell−cell adhesion (Fig. S4e, S5a). Together, these results suggested that KD may inhibit inflammatory activation of B cells and the immune response of cDC cells.

Lastly, using the CellChat, we compared signaling pathway networks among all immune cell subtypes between the KDC and NDC groups. The circle plots showed that the TGF-β signaling pathways were enhanced by KD, and the branches of endpoint to Treg cells were enriched but absent in the NDC group (Fig. 3e). The CXCL signaling pathways (from cDC cells to Th17 and γδT cells) and ICAM signaling pathways (from cDC cells to effector $CD4^+$ T and ProT cells) were enriched in NDC group but decreased in KDC group (Fig. 3f–g). Furthermore, SCENIC analysis validated that the chemotaxis signaling pathways between cDC and Th17, γδT cells were indeed weakened (Fig. 3h; Fig. S5b). As dendritic cells are crucial antigen presented cells, the chemotaxis signaling pathways associated with inflammation were also decreased between pDC and all T cell subtypes (Fig. S5c–e). These results indicated that KD could weaken the inflammatory cell–cell communications.

Ketogenic diet alleviates EAU inflammation and restores the Th17/Treg balance

To further explore the effect of KD on autoimmune diseases, we next conducted experiments on EAU, a classical animal model of uveitis. The KDE group displayed mild inflammatory infiltrate with markedly reduced clinical scores (Fig. 4a). Histopathological manifestations aligned with clinical observations (Fig. 4b), in that the KDE group showed only slight inflammatory cell infiltrations. The scRNA-seq analysis revealed a reduction of T cell ratio in the KDE (Fig. 4c).

Subsequently, we explored its regulation on specific gene expression. Compared to the ND group, the DEG numbers of KDC and KDE group were consistently concentrated in T cells and B cells (Fig. 4d). When compared to healthy control group, the NDE exhibited a high number of DEGs in T and B cells, whereas the KDE showed a low number (Fig. 4e). These downregulated genes in the KDE group were related to inflammation (*Cxcr4*, *Atf4* and *Cebpb*), MAPK signaling pathway (*Junb*, *Fos*, *Fosb*,

(See figure on next page.)

Fig. 3 Ketogenic diet induced changes in B cell transcriptional profile and immune cell–cell communications. **a** UMAP plot of B cell subsets: germinal center B cells (GBC), naïve B cells (NBC), and plasma cells (PC). **b** Heatmap exhibiting the average regulon activities of top 10 transcription factors in KDC and NDC groups, color key from white to red indicates relative expression levels from low to high. **c** Volcano plot showing upregulated and downregulated DEGs of NBC in the KDC/NDC comparison groups. Significance was determined using "FindMarkers" functions of Seurat package with Wilcoxon Rank Sum test and adjusted by Bonferroni correction. **d** Downregulated GO terms and KEGG pathways enriched in NBC cells in the KDC/NDC comparison group. Significance was calculated based on the accumulative hypergeometric distribution by Metascape webtool. **e**–**g** Circle plot showing the TGF-β signaling (**e**), CXCL signaling (**f**), ICAM signaling (**g**) of immune cell subsets in KDC and NDC groups, calculated by CellChat. The thickness of the lines represents the numbers of interaction. **h** Dotplot showing the relative expression of interaction pairs from cDC to γδT cells (left) and Th17 cells (right), respectively

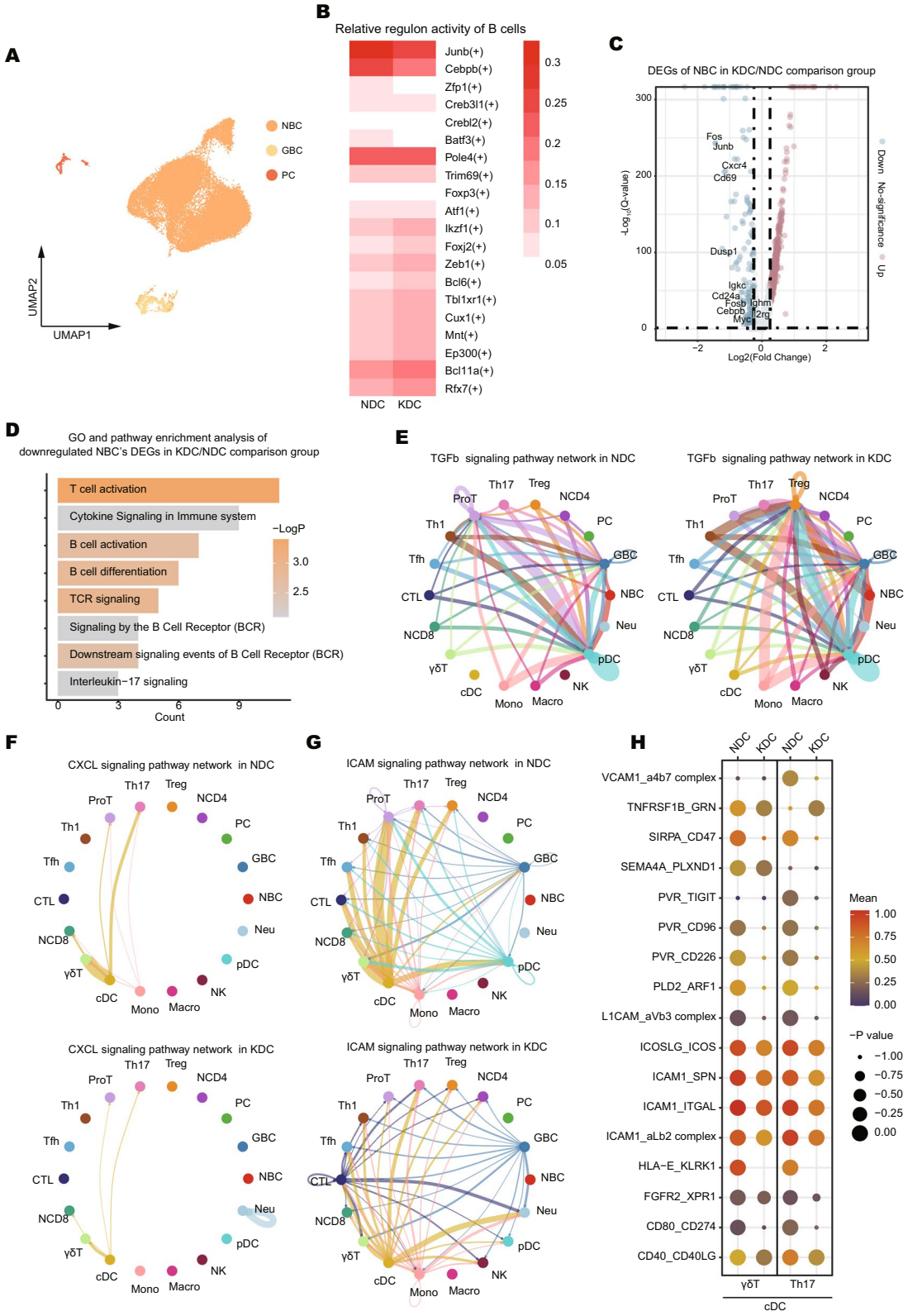

Fig. 3 (See legend on previous page.)

Jund) and Th17 cell activation (*Pim1*) (Fig. S6a). Gene function analysis of all immune cells revealed that pathways associated with cellular responses to stress, T cell activation and IL-17 signaling were downregulated in KDE group, while negative regulation of immune system process and PD−1 checkpoint pathways were upregulated (Fig. S6b-c). We also found that the IL-17 pathway was downregulated in almost all immune cell subtypes, while the AMPK pathway was upregulated (Fig. S6d). These results indicated that KD rescued the changes in gene expression caused by autoimmune responses.

Since autoimmune diseases, including uveitis, are often characterized by the aberrant differentiation of $CD4^+$ T cells [3, 42–44], we subsequently focused on these cell subsets. Based on scRNA-seq, the proportion of Th17 and Th1 cells was declined and the Treg was increased in the KDE group (Fig. 4f), consistent with the average expression levels of *Il17a* and *Foxp3* in $CD4^+$ T cells (Fig. 4g). Flow cytometry results further confirmed these findings, and the Th1 showed a declined tendency (Fig. 4h-j). Changes in splenic $CD4^+$T cell subtypes showed a consistent trend (Fig. S6e-g). Further studies found that the expression levels of T cell activation and inflammation related genes were decreased in almost all T cell subsets, especially in effector $CD4^+$ T cells (Fig. S7a). Pathways related to IL−17 signaling pathway and cell cycle were downregulated in Th17 cells, while T cell activation and proliferation were upregulated in Treg cells (Fig. S7b-c). Importantly, when $CD4^+$ T cells from the NDE and KDE mice were transferred into blank mice, respectively, the KDE group exhibited attenuated pathogenicity (Fig. S7d-e). These results demonstrated that KD effectively alleviated EAU progression and restored Th17/Treg balance.

Ketogenic diet inhibites immune cell infiltration and inflammatory response in retina

Retinal damage is the main clinical manifestation in uveitis. Therefore, we sorted the retinal immune cells for scRNA-seq to elucidate the effect of KD on local immune microenvironment. We clustered immune cells infiltrating in the retina into eight subsets, including T cells, B cells, neutrophils (Neu), monocytes and macrophages (MM), classical dendritic cells (cDC), plasmacytoid dendritic cells (pDC), microglias (MiG) and natural killer cells (NK) (Fig. 5a; Fig. S8a). The proportion of retina-infiltrating T cells also decreased after the KD (Fig. 5b). The expression of IL17 signaling-related genes (*Id2*, *Cd69* and *Pim1*) [40] and glycolysis regulatory gene (*Hif1α*) [41] were downregulated in response to KD, while genes involved in retinal development were upregulated (*Gnb1*, *Prph2*, *Pde6b*, *Prkn*) (Fig. 5c). Gene function analysis of all immune cells unveiled pathways related to regulation of cell activation, TCR signaling were downregulated; while pathways associated with negative regulation of intracellular signal transduction, myeloid cell and neutrophil apoptotic process were upregulated (Fig. S8b-c). Further subtype analysis demonstrated a significantly lower Th17 cell differentiation score in T cell and Neu subsets of the KDE group (Fig. 5d), accompanied by increased AMPK signaling pathway scores in most subtypes (Fig. S8d).

Based on scRNA-seq, the proportion of $CD4^+$T, Th17 and Th1 cells exhibited a decreased trend in the KDE group (Fig. S8f, Fig. 5f). The inflammation-related genes (*B2m* and *Pim1*) [40] and glycolysis regulatory gene (*Hif1α*) [41] were downregulated in KDE group (Fig. S8g). The pathways related to necroptotic cell death, retinal cell apoptotic process, regulation of protein catabolic process were upregulated in KDE group; while regulation of T cell activation, Th17 cell differentiation, PIP3 activates AKT signaling and TCR signaling were downregulated (Fig. S8h-i). Flow cytometry results showed that in the KDE group, the proportions of $CD4^+$ T cells and Th17 cells infiltrating in the retina were significantly reduced, the Treg cells was significantly increased, and the Th1 cells showed the declined trend (Fig. 5g–j). Additionally, using the CellChat, we compared the cell–cell

(See figure on next page.)

Fig. 4 Ketogenic diet alleviated EAU inflammation and restored the Th17/Treg balance. **a** Representative fundus images and clinical scores of eyes from the NDC, NDE and KDE group, captured on day 14 post-immunization through fundus photography. Red arrows indicate inflammatory exudation and vascular deformation. Data represented as mean ± SD. Significance was determined using one-way ANOVA. ***$P < 0.001$, ****$P < 0.0001$. **b** Representative histopathological images (hematoxylin and eosin staining) and pathological scores of retinas from the NDC, NDE and KDE group, captured on day 14 post-immunization. Red arrows indicate infiltration of inflammatory cells and retinal folding. Data represented as mean ± SD. Significance was determined using one-way ANOVA. ****$P < 0.0001$. **c** Pie charts showing the percentages of the immune cell subsets in CDLNs from NDE and KDE groups. **d** Wind rose diagrams showing the numbers of upregulated and downregulated DEGs in the KDC/NDC and KDE/NDE comparison groups. **e** Wind rose diagrams showing the numbers of upregulated and downregulated DEGs in the NDE/NDC and KDE/KDC comparison groups. **f** Pie charts showing the percentages of the T cell subsets in CDLNs from NDE and KDE groups. **G** Violin plots showing expression of *Il17a* and *Foxp3* in $CD4^+$T cells in NDE and KDE groups. **h-i** Proportions of Th17 cells (**h**), Th1 cells (**i**) and Treg cells (**j**) in CDLN $CD4^+$T cells measured by flow cytometry on day 14 post-immunization from the NDC, NDE and KDE group. Data expressed as mean ± SD. Significance was determined using one-way ANOVA. ns $P > 0.05$, *$P < 0.05$, **$P < 0.01$, ***$P < 0.001$

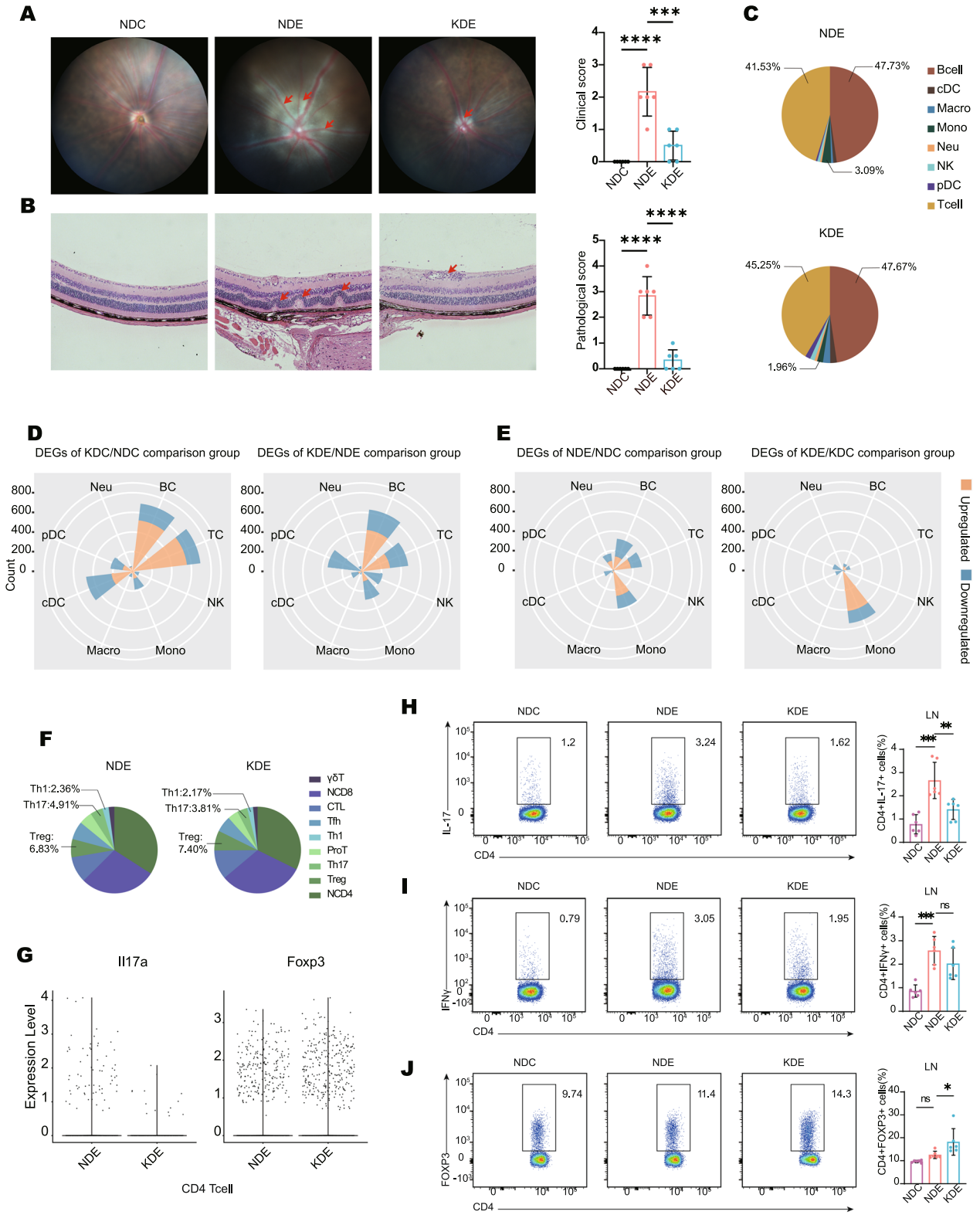

Fig. 4 (See legend on previous page.)

communication between the KDE and NDE groups. The circle plots showed that the MHC-II signaling pathways were weakened in the KDE group, while the TGF-β signaling pathways were enhanced (Fig. 5k–l). Collectively, these results suggested that KD could prevent the immune cell infiltration into the retina and mitigate the inflammatory response therein.

Integrated analysis of immune cell subsets from retina and CDLNs in KD mice

In uveitis, pathogenic immune cells in LNs migrate to the retina, altering retinal immune microenvironment [27] and causing damage. Therefore, we integrated the scRNA-seq data from retina and CDLNs (Fig. S9a), revealing significant heterogeneity (Fig. 6a). In terms of proportions, B and T cells dominated in CDLNs; while cDC, Microglia, MM, Neu and NK were more abundant in retina (Fig. 6b; Fig. S9b-c). In addition, KD simultaneously decreased the ratio of NK and T cells in retina and CDLNs. Whether in CDLNs or retina, genes related to T cell activation (*Cd69*, *Rac1*), IL17 pathway (*Il1b*, *Cebpb*), and autoimmune response (*Bhlhe40*, *Fos*, *S100a10*, *S100a13*, *S100a4*, *S100a6*) were downregulated in the KDE group, and most of them express higher levels in the retina (Fig. 6c; Fig. S9d). Multiple immune-inflammatory pathways were upregulated from LN to retina, but exhibited a mitigated tendency in the KDE group (Fig. 6d), which was same goes for immune cell subtype (Fig. S10a).

To delineate the KD's impact on evolution tendency of $CD4^+$ T cell from CDLNs to retina, we further re-clustered the merged T cell subsets (Fig. 6e) and conducted a trajectory analysis using monocle 2. The pseudotime ordering of cells were started from NCD4 to Th1_17_fh (Th17, Th1 and Tfh) and Treg cells (Fig. 6f). The CDLN $CD4^+$ T cells were mainly located at the starting pseudotime, while the retinal predominantly accumulated at the ending pseudotime, and almost no NCD4 in the retina (Fig. 6g). In addition, the retinal $CD4^+$ T cells are at a higher degree of developmental status, and KD restrain the development of Th1_17_fh (Fig. 6g). Analysis of cell ratios revealed that state 1 was dominated by NCD4 cells, both state 2 and state 3 were dominated by Th1_17_fh fate cells, with state 3 containing more Treg cells (Fig. S10b). In the KDE group, the proportion of NCD4 cells in state 1 and the Treg cells in state 3 were both upregulated, while the Th1_17_fh in state 3 was declined (Fig. S10b). Moreover, KD suppressed the expression of genes related to immunological pathways (*Cxcr4*, *Ilb2*) and IL-17 signaling (*Pim1*, *Id2*) with pseudotime (Fig. 6h–k). Together, these results suggested that retinal immune cells exhibited greater inflammatory responses than CDLN cells in uveitis, which KD could partially counteract.

Discussion

In this study, we explore the impact of KD on immune system, uncovering significant immunological changes. Specifically, KD decreases the proportion of T cells and pathways related to autoimmunity, and promotes Treg differentiation significantly at baseline. Using the EAU model, we observe that KD mitigates EAU progression by increasing Treg cell ratio, reducing Th17 cell ratio and $CD4^+$ T cell pathogenicity. Among the immune cells infiltrating the retina, KD restore the Th17/Treg balance. Analysis of integrated retinal and CDLN reveals that retinal immune cells, particularly $CD4^+$ T cells, exhibit greater inflammatory responses than CDLN cells, which KD could partially counteract.

Accumulating evidence underscores the intricate interplay between diet and the immune system [45, 46]. KD has demonstrated effectiveness in alleviating the progression of autoimmune-related diseases [5, 47, 48], yet an in-depth illustration of its immune microenvironment effects remains incomplete. In our study, we construct a comprehensive immune cell atlas of KD-mice by scRNA-seq. In healthy control mice, KD reduces T cell proportion, decreases the expression of genes related to inflammation pathway (*Fos* and *Junb*), lymphocyte activation (*Cxcr4*, *Il7r*, and *CD69*) and autoimmune disease (*Cebpb* and *Id2*). These genes are predominated in T and B cells. B cell is a kind of important immune cells, there is no clear research report on the effects of KD on it. This study shows that in B cells, KD reduces the

(See figure on next page.)

Fig. 5 Ketogenic diet inhibited immune cell infiltration and inflammatory response in retina. **a** UMAP plot clustering of retinal immune cells from NDE and KDE groups. **b** Bar chart showing the percentages of immune cell subsets in the NDE and KDE groups derived from scRNA-seq data. **c** Volcano plot showing upregulated and downregulated DEGs of all retinal infiltrating immune cells in the KDE/NDE comparison groups. Significance was determined using "FindMarkers" functions of Seurat package with Wilcoxon Rank Sum test and adjusted by Bonferroni correction. **d** Box plot showing Th17 cell differentiation scores across retinal immune subsets from NDE and KDE groups**. e** UMAP plot clustering of T cells from NDE and KDE groups. **f** Bar chart showing the percentages of T cell subsets in the NDE and KDE groups derived from scRNA-seq data. **g-j** Proportions of Th17 cells (**g**), Th1 cells (**h**), Treg cells (**i**) in retinal $CD4^+$T cells, and $CD4^+$T cells (**j**) measured by flow cytometry on day 14 post-immunization from the NDE and KDE group. Data expressed as mean ± SD. Significance was determined using one-way ANOVA. ns $P > 0.05$, $^{**}P < 0.01$, $^{****}P < 0.0001$. **k–l** Circle plot showing MHC-II signaling (**k**), TGF-β signaling (**l**) of immune cell subsets in NDE and KDE groups, calculated by CellChat. The thickness of the lines connecting cells indicates the numbers of interaction. MM: monocytes & macrophages, MiG: microglias

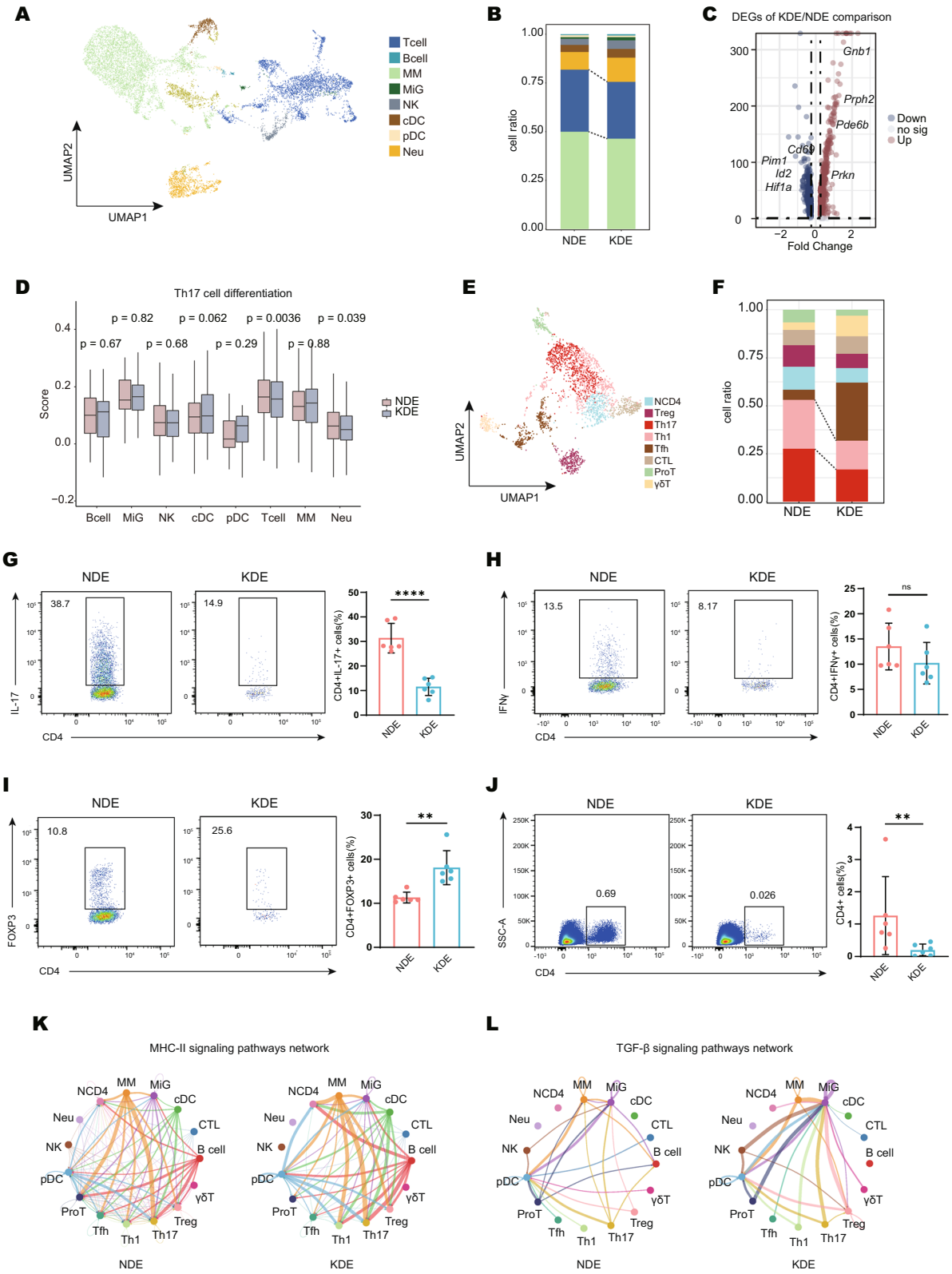

Fig. 5 (See legend on previous page.)

transcriptional activity of autoimmune related regulator, including *Junb* and *Cebpb*, while increasing the transcriptional activity of *Bcl11a* and *Rfx7* (DNA repair and anti-apoptosis regulatory molecules). B cell activation and differentiation pathway are also downregulated. In addition, KD also downregulates the inflammatory regulon activity of myeloid cells, and restrains the antigen processing and presentation function in cDC. Moreover, KD inhibits CXCL signaling pathways and enhances TGF-β signaling pathways among immune cell–cell communication. Altogether, our findings reveal that KD inhibits the expression of inflammatory gene and pathway at baseline, suggesting its potential to be a treatment option for autoimmune disease.

Uveitis, an autoimmune disorder, results in significant ocular damage, including retinal injury. The imbalance between Th17 and Treg cells is central to the disease, with pathogenic Th17 cells migrating from CDLN to retinal tissue and recruiting inflammatory cells. However, current treatments have serious systemic side effects, limited efficacy and a nonspecific nature, highlighting the urgent need for new treatments. Up to now, the effects of KD on uveitis have not been explored, and its specific impact on autoimmune diseases remains unclear. In our study, for the first time, we demonstrate that KD mitigates the disease severity in EAU via rectifying the Th17/Treg imbalance both in immune organs and retina. KD downregulates the IL-17 pathway among almost all immune cell types in LNs, while upregulating the AMPK pathway. In retina, KD decrease the expression of IL17 signaling-related genes (*Id2*, *Cd69* and *Pim1*) and glycolysis regulatory gene (*Hif1α*). Multiple immune-inflammatory related pathways are upregulated from LNs to retina, but exhibit a mitigated tendency after KD treatment. In uveitis, retinal immune cells exhibit greater inflammatory responses than LN' cells, which KD could partially counteract. Moreover, the $CD4^+$ T cells from KDE mice present a weaken pathogenicity. These results demonstrate that KD effectively alleviates EAU progression and preliminary clarify its potential mechanism.

Treg cells, which express the transcription factor Foxp3, play a central role in maintaining immune homeostasis, suppressing autoimmunity, and regulating immunity to infections and tumors [49]. TGF-β signals are indispensable for steady-state Treg cell homeostasis and for its suppression function [50]. In this study, we find that KD can promote Treg differentiation, then increase the proportion of LN' Treg cells both in healthy and EAU mice. Furthermore, the TGF-β signaling pathway are enhanced, which may partially explain why KD can correct the imbalance of Th17/Treg cells. Tailoring of Treg cell functionality occurs not only at the level of the targeted immune response, but also by the tissue site in which these cells are to function [51]. Our previous study had shown that during the development of uveitis, retinal infiltrating cells will also experience an imbalance between Th17 and Treg cells, as well as changes in corresponding inflammatory genes and pathways [52]. This study reveal that KD also increases the proportion of Treg cells in retinal infiltrating immune cells. Collectively, our findings indicates that Treg may play a crucial role in mechanisms of KD treatment.

In summary, this study provides a comprehensive exploration of KD on immune microenvironment, demonstrates the treatment role of KD on uveitis for the first time and preliminary explores the potential mechanism. Further research is needed to explore mechanisms, validate clinical applicability, and identify potential adverse effects.

Methods

Mice

Female C57BL/6 J mice of wild-type strain (6–8 weeks of age, weighing 18–25 g) were procured from the Guangzhou Animal Testing Center. All procedures followed the guidelines for animal welfare and usage. The mice were accommodated in a specific pathogen-free environment setting at 21 ± 1 °C with 60 ± 5% humidity, and maintained to a 12-h light/dark cycle. The animal experiments in our study were approved by the Institutional Animal Care Committee at Zhongshan Ophthalmic Center, Sun Yat-Sen University.

EAU model establishment

The EAU model was subcutaneously induced with human $IRBP_{1-20}$ (2 mg/mL; GiL Biochem, Shanghai,

(See figure on next page.)

Fig. 6 Merged analysis of immune cell subsets from retina and CDLNs in KD mice. **a** UMAP plot clustering of retina and CDLN immune cells from NDE and KDE groups. **b** Bar chart showing the percentages of immune cell subsets form retina and CDLN of NDE and KDE groups derived from scRNA-seq data. **c** Line charts showing the mean expression of *Pim1, Cxcr4, Hif1a, Id2* in retina and CDLN immune cells from NDE and KDE groups. **d** Representative GO terms and pathways enriched in upregulated DEGs in retina/LN comparison group between NDE and KDE groups. **e** UMAP plot clustering of retina and CDLN T cells from NDE and KDE groups. **f-g** Pseudotime trajectory analysis of $CD4^+$ T cells from retina and CDLN of NDE and KDE groups. Cells are colored by pseudotime (right), celltype (left) as indicated (**f**). Cells are colored by celltype, splited by tissues and group as indicated (**g**). **h**–**k** The scatter distribution plot showed the expression alteration of *Pim1, Cxcr4, Ilb, Id2* in each group during the pseudotime. The color coded for different tissues

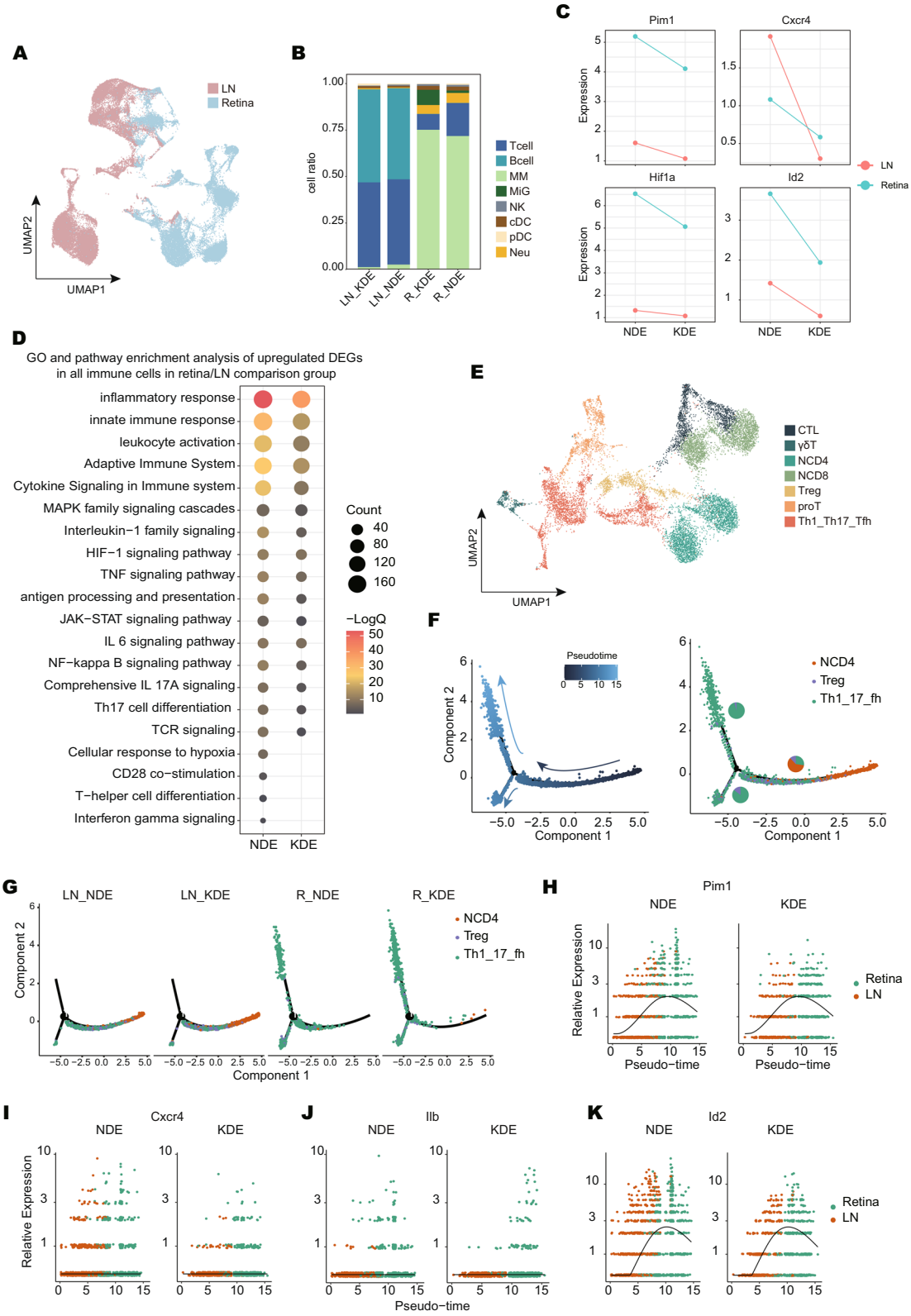

Fig. 6 (See legend on previous page.)

China) emulsified in complete Freund's adjuvant (Difco, San Jose, CA, USA) that contained 2.5 mg of Mycobacterium tuberculosis strain H37Ra (Difco) in a 1:1 volume ratio. Additionally, on days 0 and 2 post-immunization, 0.25 μg of pertussis toxin dissolved in PBS was intraperitoneally administered [53]. KD groups were treated with a 7-day adaptation to the KD, and an additional 7-day full KD regimen before EAU induction. Per group contains six mice. The exact composition of the ketogenic diet is provided in Table 1.

On day 14 after immunization, the fundus of the mice was examined and scored to evaluate EAU mice. Clinical scores ranged from 0 to 4 [54], based on observable retinal vasculitis, choroidal and retinal infiltration/lesions, papilledema, retinal hemorrhage, retinal detachment, retinal atrophy etc. (Table S1). These clinical scores were assessed in a blinded manner.

CDLN cell isolation and treatment

Cells were isolated from cervical draining lymph nodes (CDLNs) and spleen of mice for in vivo detection.

Adoptive transfer experiment

The CDLN cells from NDE and KDE mice (day 14) were cultured with IRBP1-20 (20 μg/mL), for a duration of 72 h. Subsequently, $CD4^+$ T cells were sorted (2×10^7 living cells/mouse), introducing into wild-type mice (n = 6) via tail vein injection.

Table 1 The composition of the ketogenic diet

Product	Ketogenic diet		Normal diet	
	gm%	kcal%	gm%	kcal%
Protein	16.63%	9.99%	9.56%	9.99%
Carbohydrate	0.00%	0.00%	76.50%	79.94%
Fat	66.50%	89.91%	4.24%	9.97%
Total		100		100
kcal/gm	6.7		3.8	
Ingredient	gm	kcal	gm	kcal
Casein	100.00	400	100	400
L-Cystine	1.50	6	1.5	6
		0		0
Corn starch	0.00	0	371	1484
Maltodextrin	0.00	0	35	140
Sucrose	0.00	0	406	1624
Cellulose	50.00	0	50	0
Soybean Oil	25.00	225	25	225
Cocoa butter	381.00	3429	20	180
Mineral mix S10026B	50.00	0	50	0
Vitamin mix, V10001C, 10×Vits	1.00	4	1	4
Choline Bitartrate	2.00	0	2	0
FD&C red Dye #40	0.025	0	0	0
FD&C yellow Dye #5	0.025	0	0.025	0
FD&C blue Dye #1	0	0	0.025	0
Total	610.5	4064.00	1061.5	4063

Flow cytometry

After staining with live/dead dye, the harvested cells of mice underwent surface marker staining. The cells were stained with PerCP/Cyanine5.5-anti-CD4 (Biolegend, 100,434, 0.2 μg/ml), PE/Cyanine7-anti-CD25 (Biolegend, 102,016, 0.2 μg/ml).

For intracellular staining, the cells of mice were stimulated with 5 ng/mL phorbolmyristate acetate (Sigma-Aldrich, St. Louis, MO, USA), 1 μg/mL brefeldin A (Sigma-Aldrich), and 500 ng/mL ionomycin (Sigma-Aldrich) at 37 °C for 5 h. After stimulation, the harvested mouse cells were fixed, permeabilized, stained with Alexa Fluor 647-anti-IL17A (Biolegend, 512,309, 0.2 μg/ml), Brilliant Violet 650-anti-IL-17A (Biolegend, 506,930, 0.2 μg/ml), PE-anti-IFN-γ (Biolegend, 505,808, 0.2 μg/ml), FITC-anti-Foxp3 (Invitrogen, 11-5773-82, 0.2 μg/ml), Alexa Fluor 647-anti-FOXP3 (Biolegend, 320,014, 0.2 μg/ml). Subsequently, the cells were analyzed using the BD LSRFortessa flow cytometer (BD Biosciences, San Jose, CA, USA) and the results were processed with FlowJo software version 10.0.7 (BD Biosciences).

Hematoxylin and eosin staining

Mouse eyes first underwent fixation and dehydration, and then they were paraffin-embedded and sliced into 4 μm-thick sections for staining with hematoxylin and eosin. Pathological scoring was conducted in a blinded manner according to the scoring criteria [54] (Table S1).

Polarization assays

Isolated from the cervical lymph nodes of mice using a commercial kit (Stemcell Technologies, Vancouver, BC, Canada), the purified naïve $CD4^+$T cells (2×10^5/well) were subsequently incubated with anti-CD3/CD28 beads (1 bead to 5 cells [1:5]) for 72 h in a 96-well plate. For Treg cell differentiation, the culture medium was supplemented with recombinant human IL-2 (50 U/mL, PeproTech, Rocky Hill, NJ, USA), and recombinant human TGF-β1 (10 ng/mL, PeproTech).

Isolation of CDLNs for scRNA-seq

The CDLNs were harvested from three mice per group and combined into one single sample for single-cell library preparation. After grinding, the combined cells were placed in RPMI-1640 medium (Thermo Fisher Scientific) supplemented with 2% FBS (Thermo Fisher Scientific), 3 mg/mL Collagenase IV (Sigma-Aldrich), Pen/Strep antibiotics (Thermo Fisher Scientific) and 40 mg/mL DNase I (Sigma-Aldrich). They were then incubated

at 37 °C for 15 min. Afterward, the digested cells were gathered and filtered through a 70 mm cell strainer. The resulting single-cell suspension achieved a concentration of 1×10^7 cells/mL (with a viability ≥ 85%), confirmed using the Countess® II Automated Cell Counter.

scRNA-seq data processing

ScRNA-seq libraries were generated following the manufacturer's guidelines, with slight adaptations, using the Chromium Single Cell 5' Library and Gel Bead Kit (10 × Genomics, 120,237). In detail, after wasing with 0.04% BSA buffer (0.02 g BSA dissolved in 50 ml of deionized PBS), cells were captured in droplets. Subsequently, steps including reverse transcription, emulsion breaking, barcoded-cDNA purification with Dynabeads, and PCR amplification were sequentially carried out. The amplified cDNA was then utilized to construct the 5' gene expression library. Fragmenting and end-repair, double-size selection with SPRIselect beads, and sequencing, in particular, were performed on 50 ng of amplified cDNA utilizing the NovaSeq platform (Illumina NovaSeq6000) to produce 150 bp paired-end reads. Initial processing of the sequenced data was conducted using CellRanger software v7.1.0 (10 × Genomics). Data were integrated and clustered using the Seurat package (v4.3.0) in R (v4.1.3).

For quality control, cells were filtered based on criteria of 300–4000 genes with < 15% mitochondrial genes. Cells showing high expression of Hbb-a1 and Hbb-bs, indicative of red blood cells, were also filtered out. The influence of batch effect across different samples was rectified using the Harmony package (v1.0) in R [55].

Dimensionality reduction and clustering analysis

For the analysis of scRNA-seq data, normalization was performed using the "NormalizeData" function within the Seurat package in R. Subsequently, the "FindClusters" function was employed to cluster cells and the "RunUMAP" function was utilized to visualize the data with a 2-dimensional UMAP algorithm. In addition, the "FindAllMarkers" function was used to identify marker genes for distinct clusters. Differential gene expression (DEG) across different cell types were generated using the "FindMarkers" function with Wilcoxon Rank Sum test and adjusted by Bonferroni correction. (|Log2 (fold change)| > 0.25 and adjusted *P* values < 0.05).

DEG analysis

DEG analysis across various cell types among different groups (KDE/NDE, KDC/NDC, NDE/NDC) was conducted using the 'FindMarkers' function (adjusted *P* value < 0.05, |Log2FC| > 0.25). Prior to DEG analysis, cell types that were either absent or represented by fewer than three cells in the compared groups were excluded.

Gene funtional analysis

Gene ontology (GO) and pathway enrichment analysis was conducted utilizing the Metascape webtool (www.metascape.org) [56]. The p values of GO terms are determined through the cumulative hypergeometric distribution provided by the Metascape webtool. Pathways associated with diseases were visually represented using the pheatmap (v1.0.12) and ggplot2 package (v3.2.1) in R.

Cell–cell communication

Intercellular communication analysis was conducted using the CellChat package (version 1.4.0). To uncover differential communication among immune cell types, we input the single-cell gene expression matrix and analyzed it based on the ligand-receptor data within CellChat software. This approach modeled communication probabilities and identified significant interactions. Additionally, to detect functional pathway variations, we mapped signaling changes across different cell subsets.

Trajectory analyses

Monocle 2 v2.5.4 (an R package) [57] was employed to arrange single cells along a 'pseudotime' continuum, positioning them along an inferred developmental trajectory. After quality control, genes were integrated into Monocle's Reversed Graph Embedding algorithm to sculpt this trajectory. Subsequently, Monocle executed a dimensionality reduction on the data and organized the cells along the pseudotime axis.

Statistics

Data analysis and visualization were conducted using GraphPad Prism Software v 8.0.2 (GraphPad, Inc., La Jolla, CA, USA). The results are presented as the mean ± SD. Statistical analysis was carried out employing an unpaired two-tailed Student's *t*-test, one-way ANOVA. $P < 0.05$ were considered to be statistically significant. ns, non-significant; $^{*}P < 0.05$; $^{**}P < 0.01$; $^{***}P < 0.001$; and $^{****}P < 0.0001$.

Abbreviations

CDLN	Cervical draining lymph nodes
scRNA-seq	Single-cell RNA sequencing
EAU	Experimental autoimmune uveitis
LN	Lymph node
cDC	Classical dendritic cell
pDC	Plasmacytoid dendritic cell
Neu	Neutrophil
Mono	Monocyte
Macro	Macrophage
DEG	Differentially expressed gene
NCD4	Naïve $CD4^+$ T cell
Treg	Regulatory T cells
Th17	T helper 17 cell
ProT	Proliferative T cell
Tfh	T follicular helper cell
γδT	γδT cell
CTL	CD8 + T cells with cytotoxic activity

NCD8 Naïve CD8 + T cell

Supplementary Information

The online version contains supplementary material available at https://doi.org/10.1186/s12974-024-03308-z.

Additional file 1.

Acknowledgements
The authors express their gratitude to all the study staff for their assistance and cooperation during the research.

Author contributions
W.S., L.F designed research; R.D., T.W., Z.L., L.J. and X.Y. performed research, assisted by X.L. and Z.H.; R.D., L.J., T.W., Z.L., X.Y., D.H. and T.T. analyzed data; R.D. and T.W. wrote the paper.

Funding
This study was supported by the National Outstanding Youth Science Fund Project of China (No. 82122016), Municipal School (Hospital) Jointly Fund Project of Guang Zhou (No. 2023A03J0176), China Postdoctoral Science Foundation (No. 2023M744017 and No. 2024T171071), and National Natural Science Foundation of China (No. 82070949 and No. 82271073).

Availability of data and materials
The scRNA-seq sequencing data of KD mice have been deposited in the Genome Sequence Archive at the BIG Data Center, Beijing Institute of Genomics (https://bigd.big.ac.cn/gsa/), project number: PRJCA022557; GSA accession number: CRA017594.

Declarations

Ethics approval and consent to participate
All animal tests were approved by the institutional Ethics committee (Sun Yat-Sen University).

Consent for publication
Not applicable.

Competing interests
The authors declare no competing interests.

Received: 11 July 2024 Accepted: 20 November 2024
Published online: 03 December 2024

References

1. Zarnowska IM. Therapeutic use of the ketogenic diet in refractory epilepsy: what we know and what still needs to be learned. Nutrients. 2020;12(9):2616.
2. Zhu H, Bi D, Zhang Y, et al. Ketogenic diet for human diseases: the underlying mechanisms and potential for clinical implementations. Signal Transduct Target Ther. 2022;7(1):11.
3. Krovi SH, Kuchroo VK. Activation pathways that drive CD4(+) T cells to break tolerance in autoimmune diseases(). Immunol Rev. 2022;307(1):161–90.
4. Ni FF, Li CR, Liao JX, et al. The effects of ketogenic diet on the Th17/Treg cells imbalance in patients with intractable childhood epilepsy. Seizure. 2016;38:17–22.
5. Kong C, Yan X, Liu Y, et al. Ketogenic diet alleviates colitis by reduction of colonic group 3 innate lymphoid cells through altering gut microbiome. Signal Transduct Target Ther. 2021;6(1):154.
6. Wildner G, Diedrichs-Möhring M. Resolution of uveitis. Semin Immunopathol. 2019;41(6):727–36.
7. Chong WP, Horai R, Mattapallil MJ, et al. IL-27p28 inhibits central nervous system autoimmunity by concurrently antagonizing Th1 and Th17 responses. J Autoimmun. 2014;50:12–22.
8. Direskeneli H, Fujita H, Akdis CA. Regulation of TH17 and regulatory T cells in patients with Behçet disease. J Allergy Clin Immunol. 2011;128(3):665–6.
9. Zhong Z, Su G, Kijlstra A, et al. Activation of the interleukin-23/interleukin-17 signalling pathway in autoinflammatory and autoimmune uveitis. Prog Retin Eye Res. 2021;80: 100866.
10. Zou Y, Xu S, Xiao Y, et al. Long noncoding RNA LERFS negatively regulates rheumatoid synovial aggression and proliferation. J Clin Invest. 2018;128(10):4510–24.
11. Bi X, Guo XH, Mo BY, et al. LncRNA PICSAR promotes cell proliferation, migration and invasion of fibroblast-like synoviocytes by sponging miRNA-4701-5p in rheumatoid arthritis. EBioMedicine. 2019;50:408–20.
12. Jabs DA. Immunosuppression for the uveitides. Ophthalmology. 2018;125(2):193–202.
13. Dick AD, Rosenbaum JT, Al-Dhibi HA, et al. Guidance on noncorticosteroid systemic immunomodulatory therapy in noninfectious uveitis: fundamentals of care for UveitiS (FOCUS) initiative. Ophthalmology. 2018;125(5):757–73.
14. Hu J, Wang C, Huang X, et al. Gut microbiota-mediated secondary bile acids regulate dendritic cells to attenuate autoimmune uveitis through TGR5 signaling. Cell Rep. 2021;36(12): 109726.
15. Yu J, Zhou X, Chang M, et al. Regulation of T-cell activation and migration by the kinase TBK1 during neuroinflammation. Nat Commun. 2015;6:6074.
16. Schaumburg CS, Siemasko KF, De Paiva CS, et al. Ocular surface APCs are necessary for autoreactive T cell-mediated experimental autoimmune lacrimal keratoconjunctivitis. J Immunol. 2011;187(7):3653–62.
17. Chen X, Su W, Wan T, et al. Sodium butyrate regulates Th17/Treg cell balance to ameliorate uveitis via the Nrf2/HO-1 pathway. Biochem Pharmacol. 2017;142:111–9.
18. Gasteiger G, Ataide M, Kastenmüller W. Lymph node–an organ for T-cell activation and pathogen defense. Immunol Rev. 2016;271(1):200–20.
19. Chen M, Su W, Lin X, et al. Adoptive transfer of human gingiva-derived mesenchymal stem cells ameliorates collagen-induced arthritis via suppression of Th1 and Th17 cells and enhancement of regulatory T cell differentiation. Arthritis Rheum. 2013;65(5):1181–93.
20. Louveau A, Herz J, Alme MN, et al. CNS lymphatic drainage and neuroinflammation are regulated by meningeal lymphatic vasculature. Nat Neurosci. 2018;21(10):1380–91.
21. Calder VL, Lightman SL. Experimental autoimmune uveoretinitis (EAU) versus experimental allergic encephalomyelitis (EAE): a comparison of T cell-mediated mechanisms. Clin Exp Immunol. 1992;89(2):165–9.
22. Phillips MJ, Needham M, Weller RO. Role of cervical lymph nodes in autoimmune encephalomyelitis in the Lewis rat. J Pathol. 1997;182(4):457–64.
23. Crane IJ, Liversidge J. Mechanisms of leukocyte migration across the blood-retina barrier. Semin Immunopathol. 2008;30(2):165–77.
24. Yin X, Zhang S, Lee JH, et al. Compartmentalized ocular lymphatic system mediates eye-brain immunity. Nature. 2024;628(8006):204–11.
25. Kwiatkowski AJ, Helm EY, Stewart JM, et al. Treatment with an antigen-specific dual microparticle system reverses advanced multiple sclerosis in mice. Proc Natl Acad Sci U S A. 2022;119(43): e2205417119.
26. Ataide MA, Knöpper K, de Casas PC, et al. Lymphatic migration of unconventional T cells promotes site-specific immunity in distinct lymph nodes. Immunity 2022;55(10):1813–28.e9.
27. Li H, Xie L, Zhu L, et al. Multicellular immune dynamics implicate PIM1 as a potential therapeutic target for uveitis. Nat Commun. 2022;13(1):5866.
28. Moon YM, Lee SY, Kwok SK, et al. The Fos-Related Antigen 1-JUNB/Activator Protein 1 transcription complex, a downstream target of signal transducer and activator of transcription 3, Induces T Helper 17 differentiation and promotes experimental autoimmune arthritis. Front Immunol. 2017;8:1793.
29. Wang X, Cheng W, Chen X, et al. Inhibition of CEBPB attenuates lupus nephritis via regulating Pim-1 Signaling. Mediators Inflamm. 2022;2022:2298865.
30. Kwon EK, Min CK, Kim Y, et al. Constitutive activation of T cells by γ2-herpesviral GPCR through the interaction with cellular CXCR4. Biochim Biophys Acta Mol Cell Res. 2017;1864(1):1–11.

31. Yue T, Sun F, Wang F, et al. MBD2 acts as a repressor to maintain the homeostasis of the Th1 program in type 1 diabetes by regulating the STAT1-IFN-γ axis. Cell Death Differ. 2022;29(1):218–29.
32. Wright T, Turnis ME, Grace CR, et al. Anti-apoptotic MCL-1 promotes long-chain fatty acid oxidation through interaction with ACSL1. Mol Cell. 2024;84(7):1338-53.e8.
33. Chan JD, Scheffler CM, Munoz I, et al. FOXO1 enhances CAR T cell stemness, metabolic fitness and efficacy. Nature. 2024;629(8010):201–10.
34. Delgoffe GM, Woo SR, Turnis ME, et al. Stability and function of regulatory T cells is maintained by a neuropilin-1-semaphorin-4a axis. Nature. 2013;501(7466):252–6.
35. Xu M, Pokrovskii M, Ding Y, et al. c-MAF-dependent regulatory T cells mediate immunological tolerance to a gut pathobiont. Nature. 2018;554(7692):373–7.
36. Chen L, Ke H, Zhang Y, et al. Orai1 overexpression improves sepsis-induced T-lymphocyte immunosuppression and acute organ dysfunction in mice. Heliyon. 2022;8(12): e12082.
37. Lu J, Wang X, Zhang B, et al. The lncRNA PVT1 regulates autophagy in regulatory T cells to suppress heart transplant rejection in mice by targeting miR-146a. Cell Immunol. 2021;367: 104400.
38. Weber J, de la Rosa J, Grove CS, et al. PiggyBac transposon tools for recessive screening identify B-cell lymphoma drivers in mice. Nat Commun. 2019;10(1):1415.
39. Vickridge E, Faraco CCF, Tehrani PS, et al. The DNA repair function of BCL11A suppresses senescence and promotes continued proliferation of triple-negative breast cancer cells. NAR Cancer. 2022;4(4):zcac028.
40. Hwang SM, Sharma G, Verma R, et al. Inflammation-induced Id2 promotes plasticity in regulatory T cells. Nat Commun. 2018;9(1):4736.
41. Wang H, Sun J, Sun H, et al. The OGT-c-Myc-PDK2 axis rewires the TCA cycle and promotes colorectal tumor growth. Cell Death Differ. 2024. https://doi.org/10.1038/s41418-024-01315-4.
42. Mochizuki M, Sugita S, Kamoi K. Immunological homeostasis of the eye. Prog Retin Eye Res. 2013;33:10–27.
43. Yin Y, Choi SC, Xu Z, et al. Normalization of CD4+ T cell metabolism reverses lupus. Sci Transl Med. 2015;7(274):274ra18.
44. Gomez-Bris R, Saez A, Herrero-Fernandez B, et al. CD4 T-cell subsets and the pathophysiology of inflammatory bowel disease. Int J Mol Sci. 2023;24(3):2696.
45. Alexander M, Turnbaugh PJ. Deconstructing mechanisms of diet-microbiome-immune interactions. Immunity. 2020;53(2):264–76.
46. Christ A, Lauterbach M, Latz E. Western diet and the immune system: an inflammatory connection. Immunity. 2019;51(5):794–811.
47. Bock M, Karber M, Kuhn H. Ketogenic diets attenuate cyclooxygenase and lipoxygenase gene expression in multiple sclerosis. EBioMedicine. 2018;36:293–303.
48. Goldberg EL, Asher JL, Molony RD, et al. β-Hydroxybutyrate Deactivates Neutrophil NLRP3 Inflammasome to Relieve Gout Flares. Cell Rep. 2017;18(9):2077–87.
49. Tanaka A, Sakaguchi S. Regulatory T cells in cancer immunotherapy. Cell Res. 2017;27(1):109–18.
50. Konkel JE, Zhang D, Zanvit P, et al. Transforming Growth Factor-β Signaling in Regulatory T Cells Controls T Helper-17 Cells and Tissue-Specific Immune Responses. Immunity. 2017;46(4):660–74.
51. Cipolletta D, Feuerer M, Li A, et al. PPAR-γ is a major driver of the accumulation and phenotype of adipose tissue Treg cells. Nature. 2012;486(7404):549–53.
52. Peng X, Li H, Zhu L, et al. Single-cell sequencing of the retina shows that LDHA regulates pathogenesis of autoimmune uveitis. J Autoimmun. 2024;143: 103160.
53. Yang P, Zhong Y, Du L, et al. Development and evaluation of diagnostic criteria for vogt-koyanagi-harada disease. JAMA Ophthalmol. 2018;136(9):1025–31.
54. Agarwal RK, Silver PB, Caspi RR. Rodent models of experimental autoimmune uveitis. Methods Mol Biol. 2012;900:443–69.
55. Korsunsky I, Millard N, Fan J, et al. Fast, sensitive and accurate integration of single-cell data with Harmony. Nat Methods. 2019;16(12):1289–96.
56. Zhou Y, Zhou B, Pache L, et al. Metascape provides a biologist-oriented resource for the analysis of systems-level datasets. Nat Commun. 2019;10(1):1523.
57. Qiu X, Hill A, Packer J, et al. Single-cell mRNA quantification and differential analysis with Census. Nat Methods. 2017;14(3):309–15.

Publisher's Note